Phasor Estimation in the Presence of DC Offset and CT Saturation

Soon-Ryul Nam, *Member, IEEE*, Jong-Young Park, Sang-Hee Kang, *Member, IEEE*, and
Mladen Kezunovic, *Fellow, IEEE*

Abstract—**A hybrid algorithm for phasor estimation is proposed that is immune to dc offset and current transformer (CT) saturation problems. The algorithm utilizes partial sum (PS)-based and multistage least-squares (MLS)-based methods before and after CT saturation is detected, respectively. The MLS-based method is initiated when the third difference of the secondary current detects the start point of the first saturation period. The determination of each saturation period is based on the sum of the secondary current from the start point of the first saturation period. A least-squares (LS) technique estimates the dc offset parameters from the single-cycle difference of the secondary current in the unsaturated periods. Removal of dc offset from the secondary current yields the sinusoidal waveform portion. Finally, the LS technique is used once again to estimate the phasor from the sinusoidal waveform portion. The performance of the algorithm was evaluated for a-g faults on a 345-kV 100-km overhead transmission line. The Electromagnetic Transient Program was used to generate fault current signals for different fault angles and remanent fluxes. The performance evaluation shows that the proposed algorithm accurately estimates the phasor of a current signal regardless of dc offset and CT saturation. The paper concludes by describing the hardware implementation of the algorithm on a prototype unit based on a digital signal processor.**

Index Terms—**Current transformer, dc offset, multistage least squares, saturation, partial sum, phasor estimation.**

I. INTRODUCTION

MODERN protective devices depend on knowing the phasors of the voltage and current signals. Any fault-induced dc offset must be removed from the current signal to estimate the current phasor accurately. Since a dc offset is a nonperiodic signal whose spectrum covers all frequencies, the presence of such a dc offset may result in a phasor estimation error of almost 20%, depending on the algorithm used. It is well known that the saturation of a current transformer (CT) also has an adverse influence on the estimation of the current phasor. Since dc offset itself is one of main causes of CT saturation, dc offset, and

CT saturation should be considered together when estimating the phasor of a current signal.

Over the last two decades, several techniques have been proposed to deal with the dc offset problem [1]–[9]. One approach to eliminating the effect of a dc offset is to assume a specific time constant for it. The methods in this approach, such as a Kalman filer in [1] and a digital mimic filter in [2], can completely remove the dc offset only when the time constant of the dc-offset matches the assumed one. Another approach is to estimate the dc-offset parameters. In [3] and [4], algorithms based on least squares (LS) were proposed to suppress the effect of the dc offset, which is linearized by a Taylor series expansion. LS-based algorithms can successfully suppress the effect of the dc offset over a certain range of time constants. When the time constant is small, however, their performance decreases due to the effects of the linearization. Several algorithms based on the discrete Fourier transform (DFT) have also been proposed to eliminate the effect of the dc offset. Algorithms in [5] and [6] were proposed to estimate the dc offset parameters using three successive outputs of the fundamental frequency DFT and two successive sums of single-cycle samples, respectively. Since these algorithms made use of more than one cycle samples, their response speeds were slower than other DFT-based algorithms. To cope with this drawback, [7], [8], and [9] used the output of the harmonic DFT, two partial sums of single-cycle samples, and a modified notch filter, respectively, to estimate the dc offset parameters. Although most of algorithms in these two approaches exhibit good immunity to dc offset, they do produce errors in the case of CT saturation.

Several other methods have been presented in [10]–[16] to deal with the CT saturation problem. In [10], an algorithm that estimates the magnetizing current to compensate for CT saturation was proposed. Although this algorithm is valid under various fault conditions, it requires the magnetization curve based on given CT parameters, and assumes that the remnant flux is zero before the fault occurs. Algorithms in [11] and [12] have been used to improve the accuracy of a CT, in which the initial flux is estimated and used in conjunction with the hysteresis curve to calculate the exciting current. These algorithms are based on two assumptions that the given CT has been preliminarily identified and that no dc component is present. In [13], the secondary current only in unsaturated periods is used to estimate the primary current including the dc offset, which is linearized by a Taylor series expansion. Due to this linearization, this algorithm does produce some errors, particularly when the time constant is small. An artificial neural network (ANN) has also been used to correct the distortion of secondary currents. In [14] and [15], a feedforward ANN

Fig. 1. Simplified equivalent circuit of a CT.

Fig. 2. Example of CT saturation (0° fault with 40% remanent flux).

attempts to learn the nonlinear characteristics of CT magnetization to reproduce the original waveform based on the learned characteristics. None of these methods have investigated the remnant flux in the core. In [16], a new ANN-based technique was proposed to compensate the saturated secondary current considering the presence of remnant flux in the core. Although the performance of ANN-based algorithms can be enhanced by increasing the quantity of learning data, they cannot be universally applied to different CTs because saturation effects vary even among CTs of the same type.

In a manner immune to dc offset and CT saturation, this paper proposes a hybrid algorithm that utilizes partial sum (PS)-based and multistage least squares (MLS)-based methods before and after CT saturation is detected, respectively. Evaluation of its performance shows that the proposed algorithm can estimate the phasor of a current signal with satisfactory speed and accuracy, even in the presence of dc offset and CT saturation.

The remainder of this paper is organized as follows. Section II describes the characteristics of CT saturation, and Section III provides the details of the proposed algorithm including the MLS-based method. Section IV presents the results of performance evaluation regarding the response speed and accuracy under various fault angles and remanent fluxes. Section V describes how the algorithm was implemented on a digital signal processor (DSP)-based prototype unit and concluding remarks are given in Section VI.

II. CHARACTERISTICS OF CT SATURATION

Modern microprocessor-based protective devices have very low impedances as seen by CTs and can be neglected when considering CT saturation. The CT wire resistance and the resistance of the leads that interconnect CTs and protective devices are the major causes for CT saturation. Fig. 1 shows a simplified equivalent circuit of a CT, where L_M is the magnetization inductance, R is the total secondary resistance, i_P is the primary current referred to the secondary, i_M is the magnetizing current, and i_S is the secondary current.

The core flux λ is related to i_S by the expression

$$\frac{d\lambda(t)}{dt} = R \cdot i_S(t) \tag{1}$$

Integrating (1) from t_0 to t yields

$$\lambda(t) = \lambda(t_0) + R \cdot \int_{t_0}^{t} i_S(\tau)\, d\tau \tag{2}$$

Assuming that a fault occurs at a time origin, and that the fault current signal consists of a dc offset and a fundamental frequency component, the discrete primary current is expressed as

$$i_P[n] = i_{ac}[n] + i_{dc}[n]$$
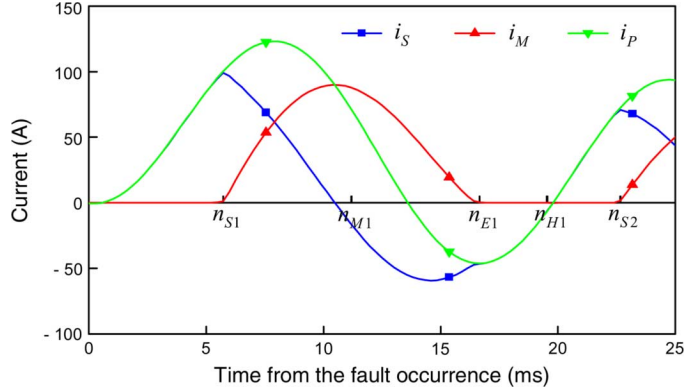
$$= A\cos(n\theta_\Delta) + B\sin(n\theta_\Delta) + C\alpha^n \tag{3}$$

where

$$\alpha = e^{-\frac{\Delta t}{\tau}}, \quad \Delta t = \frac{2\pi}{\omega}\frac{1}{N}, \quad \theta_\Delta = \omega \cdot \Delta t$$

where
- ω angular fundamental frequency;
- τ time constant of the dc offset;
- N number of samples per system cycle.

Since the primary current is equal to the sum of the secondary current and the magnetizing current, the secondary current is given by

$$i_S[n] = i_P[n] - i_M[n] = i_{ac}[n] + i_{dc}[n] - i_M[n] \tag{4}$$

To eliminate i_{ac} from i_S of (4), a single-cycle difference function is defined as

$$\begin{aligned} i_D[n] &= i_S[n-N] - i_S[n] \\ &= (i_{dc}[n-N] - i_{dc}[n]) \\ &\quad + (i_M[n-N] - i_M[n]). \end{aligned} \tag{5}$$

Fig. 2 shows an example of CT saturation, where n_{S_k} and n_{E_k} are, respectively, the start and end points of the kth saturation period brought into focus, n_{M_k} is the middle point between n_{S_k} and n_{E_k}, and n_{H_k} is the point half a cycle later than n_{M_k}. With H defined as the minimum half-length of unsaturated periods, the minimum data number in the unsaturated periods is given by $2H + 1$. For example, assuming that the maximum saturation period is less than 90% of one cycle and that the sampling rate is set to 64 samples per cycle, H will be equal to 2. In this case, i_S should be unsaturated at least from $n_{H_k} - 2$ to $n_{H_k} + 2$. Therefore, i_M should be zero within a distance H from n_{H_k}

$$i_M = 0 \quad \text{for } |n - n_{H_k}| \leq H. \tag{6}$$

Similarly, i_M should be also zero within a distance H from $n_{H_k} - N$

$$i_M = 0 \quad \text{for } |n - (n_{H_k} - N)| \leq H. \tag{7}$$

Combining (5), (6), and (7) yields

$$i_D[n] = i_{dc}[n-N] - i_{dc}[n]$$

$$= C\alpha^{n-N}(1 - \alpha^N) \quad \text{for} \quad |n - n_{H_k}| \leq H. \quad (8)$$

III. HYBRID ALGORITHM FOR PHASOR ESTIMATION

A. PS-Based Method [8]

The PS-based method is one of the most useful techniques for removing the effect of a dc offset. It is described briefly below. The phasor from the conventional DFT is given by

$$\mathbf{I}_{\text{DFT}}[n] = I_C[n] + j \cdot I_S[n] \quad (9)$$

where

$$I_C[n] = \frac{2}{N} \sum_{m=0}^{N-1} i_L[n - N + 1 + m] \cdot \cos(m\theta_\Delta)$$

$$I_S[n] = -\frac{2}{N} \sum_{m=0}^{N-1} i_L[n - N + 1 + m] \cdot \sin.(m\theta_\Delta).$$

To remove the effect of the dc offset, two partial sums are defined as

$$S_1[n] = \sum_{m=1}^{N/2} i_L[n - N - 1 + 2m] \quad (10)$$

$$S_2[n] = \sum_{m=1}^{N/2} i_L[n - N + 2m]. \quad (11)$$

Using these partial sums, the compensated real and imaginary parts are given by

$$I_R[n] = I_C[n] + \left(1 - \alpha \cos\left(\frac{2\pi}{N}\right)\right) C(\alpha)S_1[n] \quad (12)$$

$$I_I[n] = I_S[n] - \alpha \sin\left(\frac{2\pi}{N}\right) C(\alpha)S_1[n] \quad (13)$$

where

$$C(\alpha) = \frac{2}{N} \cdot \frac{\alpha^2 - 1}{\alpha^2 - 2\alpha \cos\left(\frac{2\pi}{N}\right) + 1}, \quad \alpha = \frac{S_2[n]}{S_1[n]}.$$

Finally, the PS-based phasor is given by

$$\mathbf{I}_{\text{PS}}[n] = I_R[n] + j \cdot I_I[n]. \quad (14)$$

As shown in Fig. 3, the PS-based method performs better than the conventional DFT in the presence of dc offset with no CT saturation. However, when the secondary current is distorted due to CT saturation as shown in Fig. 4, the PS-based method produces some errors as does the conventional DFT. To cope with this drawback, a MLS-based method will be proposed in this paper. Since the PS-based method performs well except in the presence of CT saturation, the PS-based method is used primarily, and the MLS-based method is applied only in the presence of CT saturation. The flowchart of the algorithm is shown in Fig. 5.
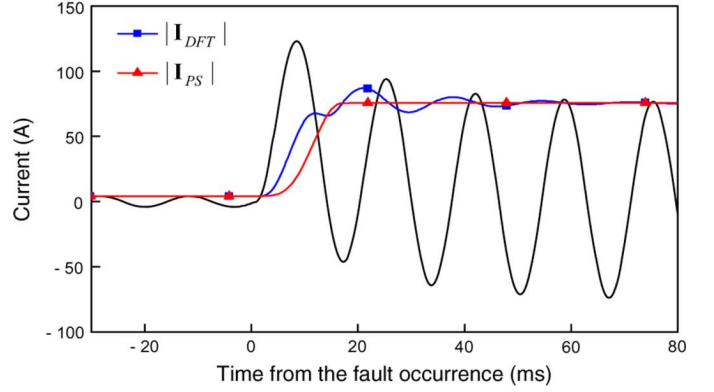
Fig. 3. Time responses of the conventional DFT and the PS-based method in the case of no CT saturation (0° fault with 40% remanent flux).
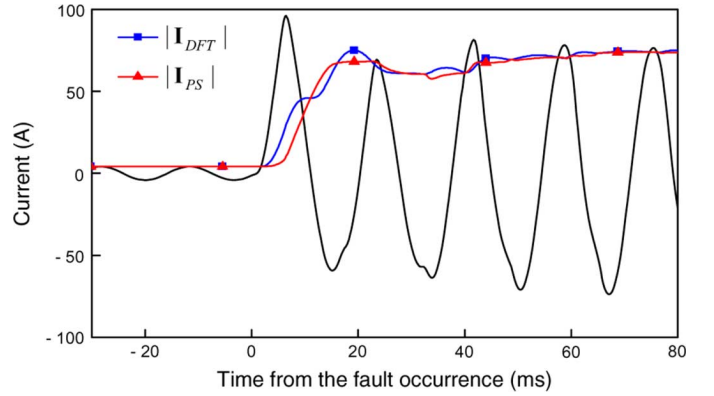
Fig. 4. Time responses of the conventional DFT and the PS-based method in the case of CT saturation (0° fault with 40% remanent flux).
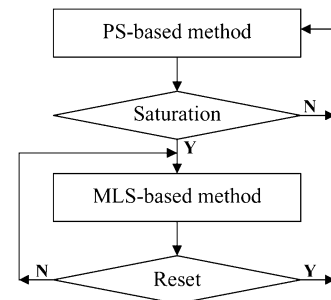
Fig. 5. Flowchart of the hybrid algorithm.

B. Detection of the Start Point of the First Saturation Period

To detect the start point of the first saturation period denoted as n_{S1}, the third difference function proposed in [17] is used, and the detection criterion is given by

$$|i_S[n] - 3i_S[n - 1] + 3i_S[n - 2] - i_S[n - 3]| > T_S. \quad (15)$$

T_S is the threshold value which can be determined using

$$T_S = k\sqrt{2}I_{\max}\left[2\sin\left(\frac{\pi}{N}\right)\right]^3 \qquad (16)$$

where $I_{\max}$ is the expected maximum fault current and k is a marginal factor. The first moment satisfying (16) is considered to be the start point of the first saturation period. To prevent malfunction, saturation detection is not applied until the initiation point, which is denoted as n_I and defined as the moment when the current first exceeds twice the rated secondary current for three successive samples.

C. MLS-Based Method

1) Determination of Estimation Points: The core flux λ of (2) can be expressed in discrete form as

$$\lambda[n] = \lambda[n_{S1}] + \frac{2\pi}{N\omega}R$$
$$\times \sum_{m=n_{S1}+1}^{n} i_S[m] \quad \text{for } n > n_{S1} \quad (17)$$

where n_{S1} corresponds to t_0 of (2). Once n_{S1} is detected by (15), the direction of saturation can be determined based on the sign of $i_S[n_{S1}]$. A positive value of $i_S[n_{S1}]$ means that $\lambda[n_{S1}]$ also has a positive value, and that the saturation occurs while $\lambda[n]$ is larger than $\lambda[n_{S1}]$. Conversely, a negative value of $i_S[n_{S1}]$ means that $\lambda[n_{S1}]$ also has a negative value, and that the saturation occurs while $\lambda[n]$ is smaller than $\lambda[n_{S1}]$. Therefore, the criterion for a saturation period can be expressed as

$$\frac{i_S[n_{S1}]}{|i_S[n_{S1}]|}\lambda[n] \ge \frac{i_S[n_{S1}]}{|i_S[n_{S1}]|}\lambda[n_{S1}] \quad \text{for } n > n_{S1}. \qquad (18)$$

Substituting (17) into (18) with minor calculation yields

$$S[n] = \frac{i_S[n_{S1}]}{|i_S[n_{S1}]|}\sum_{m=n_{S1}+1}^{n} i_S[m] \ge 0 \quad \text{for } n > n_{S1}. \qquad (19)$$

While $S[n]$ has a positive value in a saturation period, $S[n]$ has a negative value in an unsaturated period. Therefore, for the kth saturation period, the start point n_{S_k} and the end point n_{E_k} can be easily determined by examining $S[n]$.

In this paper, the dc offset parameters are estimated only at a specific point in each saturation period. Since the parameter estimation uses the single-cycle difference function and a data window of length $2H+1$, the estimation point is given by

$$n_{P_k} = n_{M_k} + N/2 + H = n_{H_k} + H. \qquad (20)$$

2) Parameter Estimation of DC Offset: At the estimation point, the LS technique is used to estimate the dc offset parameters. To fit the exponential dc offset of (8), the absolute value function and logarithm are successively applied to both sides of (8) to give

$$\log(|i_D[n]|) = n\log(\alpha) + \log(|C|\alpha^{-N}(1-\alpha^N))$$

$$\text{for} \quad |n - n_{H_k}| \le H. \qquad (21)$$

LS fitting proceeds by finding the sum of the squares regarding the deviations in $2H+1$ data from (21):

$$E_1 = \sum_{m=-H}^{H}(\log(|i_D[n_{H_k}+m]|) - p\cdot m - q)^2 \qquad (22)$$

where

$$p = \log(\alpha)$$
$$q = \log(|C|\alpha^{-N}(1-\alpha^N)) + n_{H_k}\cdot\log(\alpha).$$

The best-fit values are determined by minimizing (22), which leads to the following equations:

$$p\sum_{m=-H}^{H}m^2 + q\sum_{m=-H}^{H}m$$
$$= \sum_{m=-H}^{H}m\log(|i_D[n_{H_k}+m]|) \qquad (23)$$

$$q\sum_{m=-H}^{H}1 + p\sum_{m=-H}^{H}m$$
$$= \sum_{m=-H}^{H}\log(|i_D[n_{H_k}+m]|). \qquad (24)$$

Some minor calculation yields α and C

$$\alpha = e^p \qquad (25)$$
$$C = \frac{i_{\text{dc}}[n_{P_k}]}{|i_{\text{dc}}[n_{P_k}]|}\cdot e^q\cdot\alpha^{-n_{H_k}}\cdot\frac{\alpha^N}{1-\alpha^N} \qquad (26)$$

where

$$p = \left(\sum_{m=-H}^{H}m\log(|i_D[n_{H_k}+m]|)\right)\bigg/\left(\sum_{m=-H}^{H}m^2\right)$$
$$q = \frac{1}{2H+1}\sum_{m=-H}^{H}\log(|i_D[n_{H_k}+m]|).$$

3) MLS-Based Phasor: As noted in Section II, i_M should be zero during the periods when $|n - (n_{H_k} - N)| \le H$ and $|n - n_{H_k}| \le H$. Therefore, the sinusoidal waveform portion can be directly obtained by eliminating the dc offset from the secondary current

$$i_{\text{ac}}[n] = i_S[n] - i_{\text{dc}}[n] = i_S[n] - C\cdot\alpha^n$$
$$\text{for } |n - (n_k - N)| \le H \quad \text{and} \quad |n - n_k| \le H. \quad (27)$$

The LS technique is used once again for phasor estimation. Considering the phase relation to the PS-based phasor, the error function is

$$E_2 = e[n_{H_k}] + e[n_{H_k} - N] \qquad (28)$$

where

$$e[n] = \sum_{m=-H}^{H} \begin{pmatrix} i_{ac}[n+m] \\ -A\cos((m-M-1)\theta_\Delta) \\ +B\sin((m-M-1)\theta_\Delta). \end{pmatrix}^2$$

Minimizing (28) yields the best-fit values in the following matrix form:

$$\mathbf{x} = \mathbf{A}^{-1}\mathbf{b} \qquad (29)$$

where we get the equation shown at the bottom of the page. Finally, the MLS-based phasor is given by

$$\mathbf{I}_{MLS}[n_{P_k}] = I_R[n_{P_k}] + j \cdot I_I[n_{P_k}]. \qquad (30)$$

D. Phasor Estimation Process

Until the next estimation point, the phasor of the hybrid algorithm is given by

$$\mathbf{I}_{HA}[n] = \mathbf{I}_{MLS}[n_{P_k}]e^{j(n-n_{P_k})\theta_\Delta} \quad \text{for } n \geq n_{P_k}. \qquad (31)$$

As shown in the flowchart of Fig. 3, the MLS-based method is applied only in the presence of CT saturation. If no saturation is detected until the second zero-crossing point from the end point of the previous saturation period, the hybrid algorithm is reset, and the phasor of the algorithm comes from the PS-based method again.

IV. PERFORMANCE EVALUATION

The performance of the algorithm was evaluated for a-g faults on a 345-kV 100-km overhead transmission line as shown in Fig. 6. The overhead transmission line parameters used in the simulations are given in Table I. The Electromagnetic Transient Program (EMTP) was used to generate fault current signals for different fault angles and different remanent fluxes. The sampling frequency was set to 3840 Hz or 64 samples per cycle in 60-Hz systems. The EMTP output was pre-conditioned by a second-order Butterworth low-pass filter with a cutoff frequency of 960 Hz to reject high frequency components and prevent aliasing errors. The a-g faults incepted at four different angles (0°, 45°, 90°, and 135°) were considered to occur at a distance of 5 km from a relaying point.
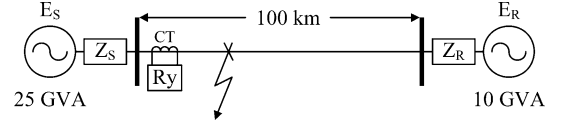
Fig. 6. Single line diagram of the model system.

TABLE I
OVERHEAD TRANSMISSION LINE PARAMETERS

Sequence	Parameter	Value	Unit
Positive	R_1, R_2	0.0345	Ω/km
&	L_1, L_2	0.9724	mH/km
Negative	C_1, C_2	0.0117	$\mu F/km$
	R_0	0.2511	Ω/km
Zero	L_0	2.7058	mH/km
	C_0	0.0045	$\mu F/km$
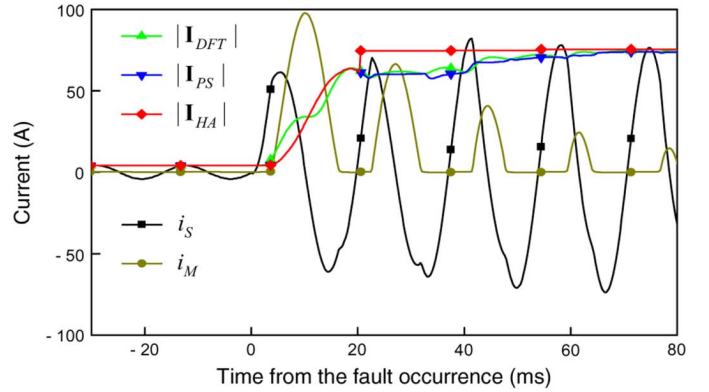
Fig. 7. Time responses for a 0° fault with 80% remanent flux.

Different remanent fluxes in the core produce different secondary currents for the same fault. Thus, the performance of the algorithm was also tested by varying the remanent flux from −80% to 80% of the flux at the saturation point. The CT modeling method in [18] was used to account for the remanent flux at the moment of energization. A resistive burden of 3.42 Ω was connected to a C400 CT (2000:5, 0.61 Ω) and the saturation point of (2.047 A, 1.512 Vs) was selected to generate hysteresis data using HYSDAT, an auxiliary program in EMTP.

To account for the delay time in the low-pass filter and to exclude data before the occurrence of the fault, the estimation point of (20) was modified for the simulations to

$$n_{P_k} = \max(n_{M_k} + N/2 + H, \, n_I + N + 2H)$$

$$\mathbf{x} = [I_R[n_{P_k}] \quad I_I[n_{P_k}]]^T$$

$$\mathbf{A} = \begin{bmatrix} 2\sum_{m=-H}^{H}\cos^2((m-H-1)\theta_\Delta) & -\sum_{m=-H}^{H}\sin(2(m-H-1)\theta_\Delta) \\ \sum_{m=-H}^{H}\sin(2(m-H-1)\theta_\Delta) & -2\sum_{m=-H}^{H}\sin^2((m-H-1)\theta_\Delta) \end{bmatrix}$$

$$\mathbf{b} = \begin{bmatrix} \sum_{m=-H}^{H}(i_{ac}[n_{H_k}+m] + i_{ac}[n_{H_k}-N+m])\cos((m-H-1)\theta_\Delta) \\ \sum_{m=-H}^{H}(i_{ac}[n_{H_k}+m] + i_{ac}[n_{H_k}-N+m])\sin((m-H-1)\theta_\Delta) \end{bmatrix}.$$
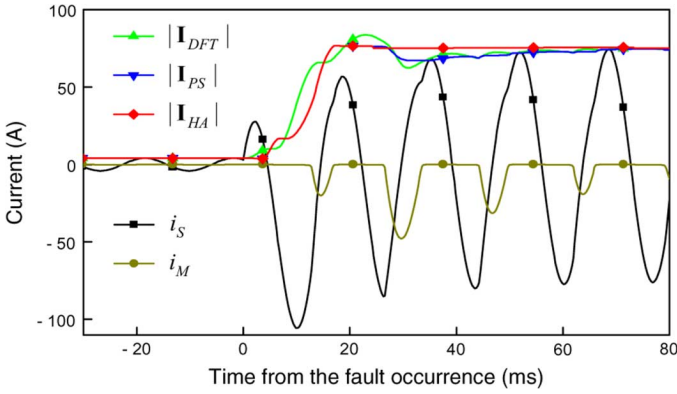
Fig. 8. Time responses for a 135° fault with 40% remanent flux.

$$= n_{H_k} + H. \tag{32}$$

Since the 0° a-g fault with 80% remanent flux is the worst case among those simulated, the first saturation period in this case becomes the maximum saturation period, which is about 82% of one cycle. Therefore, the minimum half-length of the unsaturated periods is about five samples. However, considering the effect of the low-pass filter and the residual magnetizing current, H was set to 2 for the simulations.

Fig. 7 shows the time responses of the conventional DFT, the PS-based method, and the proposed algorithm for the 0° fault with 80% remanent flux. Fig. 8 shows the same for the 135° fault with 40% remanent flux. As expected, the conventional DFT and the PS-based method required much longer time than the hybrid algorithm to reach steady state after a fault. To evaluate the response speed of the algorithms, we defined convergence time as the amount of time required for the transient oscillations to stay within ±5% of the steady-state value after a fault. Table II summarizes the convergence times of the conventional DFT, the PS-based method, and the hybrid algorithm. Depending on the fault angle and the remanent flux, the conventional DFT and the PS-based method exhibited a convergence time between 13.5 and 59.9 ms. This range is enough to cause a malfunction of protective devices that use currents as input signals. Compared to the conventional DFT and the PS-based method, the hybrid algorithm showed a much faster response with a convergence time between 12.2 and 23.2 ms.

Fig. 9 shows the real and imaginary parts of the hybrid algorithm output for the 0° fault with 80% remanent flux. Due to the switch from the PS-based method to the MLS-based method, both of the real and imaginary parts have prominent distortions at about 20.6 ms from the onset of the fault, which results in the discontinuity in the phase domain. In the case of the 135° fault with 40% remanent flux, the switch between the methods took place smoothly at about 24.5 and 115 ms, as shown in Fig. 10. The difference between the two cases is due to the saturation level at the moment of switching. Comparison of the magnetizing currents in Fig. 7 and 8 indicates that in the case of the 0° fault with 80% remanent flux, a much higher saturation level occurs at the first switching moment than in the case of the 135° fault with 40% remanent flux.

TABLE II
CONVERGENCE TIMES OF THE CONVENTIONAL DFT, THE PS-BASED METHOD, AND THE PROPOSED ALGORITHM

(Unit: ms)

	Fault Angle	Remanent Flux				
		80%	40%	0%	-40%	-80%
$\mathbf{I}_{DFT}$	0°	59.89	59.89	59.89	59.89	59.63
	45°	57.29	57.03	57.03	57.03	57.03
	90°	22.40	21.61	14.58	14.58	14.58
	135°	34.63	45.83	45.83	45.83	45.83
$\mathbf{I}_{PS}$	0°	59.89	59.89	59.89	59.89	59.89
	45°	57.55	57.55	57.55	57.55	57.55
	90°	22.92	22.39	13.54	13.54	13.54
	135°	16.41	50.26	50.26	50.26	50.26
$\mathbf{I}_{HA}$	0°	20.31	21.09	21.09	13.28	13.28
	45°	19.01	19.53	14.32	12.24	12.76
	90°	18.49	19.27	13.54	13.54	13.54
	135°	16.41	15.62	15.36	23.18	22.39
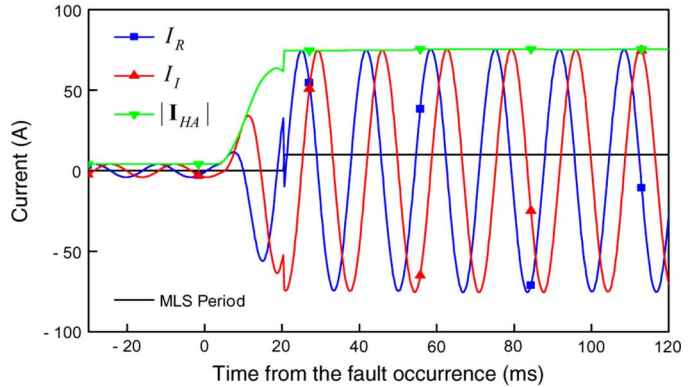
Fig. 9. Real and imaginary parts of the proposed algorithm output for a 0° fault with 80% remanent flux.
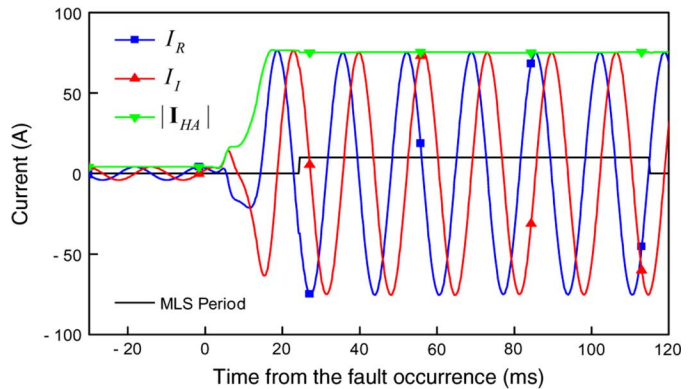
Fig. 10. Real and imaginary parts of the proposed algorithm output for a 135° fault with 40% remanent flux.

To evaluate the accuracy of the algorithms, the estimation error is calculated using the following equation:

$$\text{error} = \frac{|\text{estimated magnitude} - \text{actual magnitude}|}{\text{actual magnitude}} \times 100 \tag{33}$$

TABLE III
MAXIMUM ERRORS OF THE CONVENTIONAL DFT, THE PS-BASED METHOD,
AND THE PROPOSED ALGORITHM

(Unit: %)

	Fault Angle	Remanent Flux				
		80%	40%	0%	-40%	-80%
$\mathbf{I}_{DFT}$	0°	19.75	19.69	20.87	23.49	26.97
	45°	16.04	15.93	17.22	19.62	22.36
	90°	1.467	0.901	0.280	0.234	0.232
	135°	12.71	17.16	15.19	13.29	16.09
$\mathbf{I}_{PS}$	0°	23.66	23.47	23.11	23.46	23.18
	45°	18.65	18.36	17.94	18.63	14.65
	90°	4.377	3.080	0.677	0.099	0.108
	135°	4.752	10.85	14.79	14.30	16.04
$\mathbf{I}_{HA}$	0°	1.022	0.547	0.406	0.350	0.352
	45°	1.845	0.603	0.603	0.603	0.603
	90°	0.266	0.663	0.677	0.099	0.108
	135°	2.797	0.527	0.465	0.444	0.972
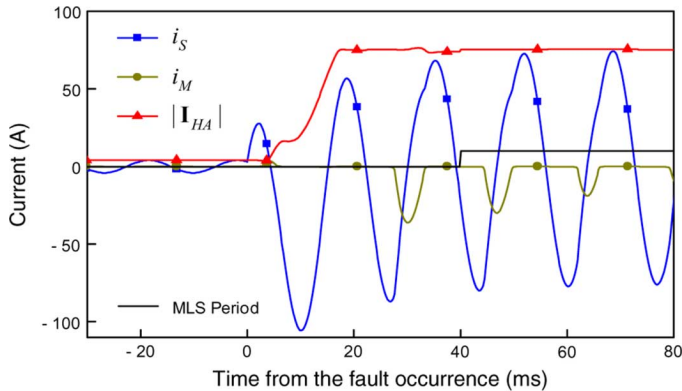
Fig. 11.   Time responses for a 135° fault with 80% remanent flux.
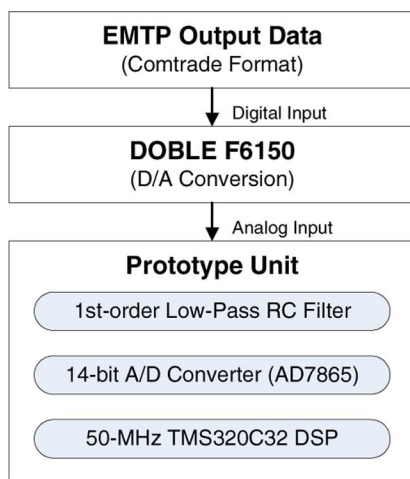
Fig. 12.   Block diagram of the hardware implementation.

where the actual magnitude of the steady-state fault current is known from a fault analysis. Table III summarizes the maximum errors after one and a half cycles following the fault occurrence. Compared to the conventional DFT and the PS-based
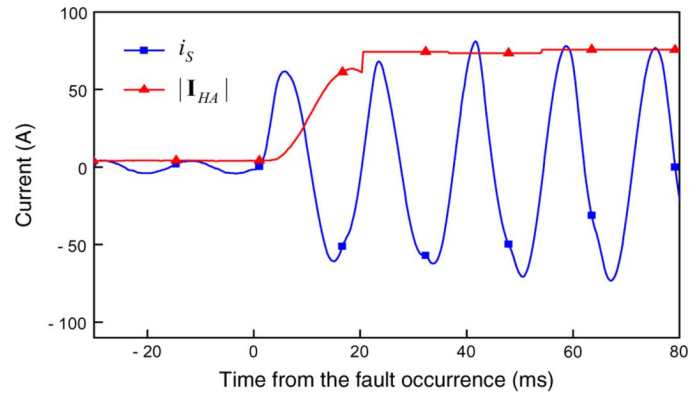
Fig. 13.   Result of the hardware test for a 0° fault with 80% remanent flux.

method, which had maximum errors between 0.11 and 27.0%, the proposed algorithm estimated the phasor more accurately with a maximum error between 0.11 and 2.80 %. The proposed algorithm produced the largest maximum error in the case of the 135° fault with 80% remanent flux. As Fig. 11 shows, the switch from the PS-based method to the MLS-based method occurred at about 40 ms after the fault occurrence, due to the very low saturation level just after the fault occurrence. Consequently, the PS-based method produced the largest maximum error during the period between the fault occurrence and the moment of switching.

These results demonstrated that the performance of the algorithm is reliable for various fault angles and remanent fluxes.

V. HARDWARE IMPLEMENTATION

The proposed algorithm was implemented on a 50-MHz TMS320C32 DSP-based prototype unit. The implemented hardware was tested using the system configuration shown in Fig. 12. The sampling rate was 64 samples per cycle and the current passed through a first-order low-pass RC filter, with a cutoff frequency of 960 Hz, to the 14-bit A/D converter.

The time responses of the algorithm from the hardware and simulation tests were almost identical, except that there are slightly more errors in the hardware tests. For example, Fig. 13 shows how the prototype unit performed when tested using the data for the 0° fault with 80% remanent flux. For this case, the maximum error was approximately 2.404% and 1.022% in the hardware and simulation tests, respectively. Similar results were found in the other hardware tests. The results indicate that a prototype unit can accurately estimate the phasor of a current signal in real time.

VI. CONCLUSION

This paper proposed a hybrid algorithm that utilizes the PS-based and MLS-based methods before and after CT saturation is detected, respectively. Since the PS-based method performs well except in the presence of CT saturation, the PS-based method is used primarily, and the MLS-based method is initiated when the third difference of the secondary current detects the start point of first saturation period. The LS technique estimates the dc offset parameters from the single-cycle

difference of the secondary current in the unsaturated periods. After the sinusoidal waveform portion is obtained by eliminating the dc offset from the secondary current, the LS technique is used one more for phasor estimation.

The performance of the algorithm was evaluated for a-g faults on a 345-kV 100-km overhead transmission line. The results show that the proposed algorithm operates reliably with a convergence time in the range of $12.2\sim23.2$ ms, and with a maximum error in the range of $0.11\sim2.80\%$ after one and a half cycles from the onset of the fault. In addition, a prototype unit estimated the phasor of a current signal successfully when the algorithm was implemented on a TMS320C32 DSP. Therefore, the hybrid algorithm is considered useful for phasor estimation immune to dc offset and CT saturation.

REFERENCES

[1] G. Benmouyal, "Frequency-doman characterization of kalman filters as applied to power system protection," *IEEE Trans. Power Del.*, vol. 7, no. 3, pp. 1129–1138, Jul. 1992.

[2] G. Benmouyal, "Removal of DC offset in current waveforms using digital mimic filtering," *IEEE Trans. Power Del.*, vol. 10, no. 2, pp. 621–630, Apr. 1995.

[3] A. Isaksson, "Digital protective relaying through recursive least-squares identification," *Proc. Inst. Elect. Eng., Gen., Transm. Distrib.*, vol. 135, no. 5, pp. 441–449, Sept. 1988.

[4] M. S. Sachdev and M. Nagpal, "A recursive least error squares algorithm for power system relaying and measurement applications," *IEEE Trans. Power Del.*, vol. 6, no. 3, pp. 1008–1015, Jul. 1991.

[5] J.-C. Gu and S.-L. Yu, "Removal of DC offset in current and voltage signals using a novel Fourier filter algorithm," *IEEE Trans. Power Del.*, vol. 15, no. 1, pp. 73–79, Jan. 2000.

[6] E. Rosolowski, J. Izykowski, and B. Kasztenny, "Adaptive measuring algorithm suppressing a decaying DC component for digital protective relays," *Elect. Power Syst. Research*, vol. 60, no. 2, pp. 99–105, Dec. 2001.

[7] T. S. Sidhu, X. Zhang, F. Albasri, and M. S. Sachdev, "Discrete-Fourier-transform-based technique for removal of decaying DC offset from phasor estimates," *Proc. Inst. Elect. Eng., Gen., Transm. Distrib.*, vol. 150, no. 6, pp. 745–752, Nov. 2003.

[8] Y. Guo, M. Kezunovic, and D. Chen, "Simplified algorithms for removal of the effect of exponentially decaying DC offset on the Fourier algorithm," *IEEE Trans. Power Del.*, vol. 18, no. 3, pp. 711–717, Jul. 2003.

[9] S. R. Nam, J. M. Sohn, S. H. Kang, and J. K. Park, "Modified notch filter-based instantaneous phasor estimation for high-speed distance protection," *Elect. Eng.*, vol. 89, no. 4, pp. 311–317, Mar. 2007.

[10] Y. C. Kang, J. K. Park, S. H. Kang, A. T. Johns, and R. K. Aggarwal, "An algorithm for compensating secondary currents of current transformers," *IEEE Trans. Power Del.*, vol. 12, no. 1, pp. 116–124, Jan. 1997.

[11] N. Locci and C. Musoas, "A digital compensation method for improving current transformer accuracy," *IEEE Trans. Power Del.*, vol. 15, no. 4, pp. 1104–1109, Oct. 2000.

[12] N. Locci and C. Muscas, "Hysteresis and eddy currents compensation in current transformers," *IEEE Trans. Power Del.*, vol. 16, no. 2, pp. 154–159, Apr. 2001.

[13] P. Jiuping, K. Yu, and Y. Hu, "An efficient compensation algorithm for current transformer saturation effects," *IEEE Trans. Power Del.*, vol. 19, no. 4, pp. 1623–1628, Oct. 2004.

[14] D. C. Yu, J. C. Cummins, Z. Wang, H.-J. Yoon, L. A. Kojovic, and D. Stone, "Neural network for current transformer saturation correction," in *Proc. IEEE Transmission Distribution Conf.*, New Orleans, LA, Apr. 1999.

[15] D. C. Yu, J. C. Cummins, Z. Wang, H.-J. Yoon, and L. A. Kojovic, "Correction of current transformer distorted secondary currents due to saturation using artificial neural networks," *IEEE Trans. Power Del.*, vol. 16, no. 2, pp. 189–194, Apr. 2001.

[16] H. Khorashadi-Zadeh and M. Sanaye-Pasand, "Correction of saturated current transformers secondary current using ANNs," *IEEE Trans. Power Del.*, vol. 21, no. 1, pp. 73–79, Jan. 2006.

[17] Y. C. Kang, S. H. Ok, and S. H. Kang, "A CT saturation detection algorithm," *IEEE Trans. Power Del.*, vol. 19, no. 1, pp. 78–85, Jan. 2004.

[18] M. Kezunovic, L. Kojovic, A. Abur, C. W. Fromen, and F. Phillips, "Experimental evaluation of EMTP-based current transformer models for protective relay transient study," *IEEE Trans. Power Del.*, vol. 9, no. 1, pp. 405–413, Jan. 1994.

Soon-Ryul Nam (S'96–M'02) received the B.S., M.S., and Ph.D. degrees from Seoul National University, Seoul, Korea, in 1996, 1998, and 2002, respectively.

Currently, he is an Assistant Professor at Myongji University, Yongin, Korea. He was with Hoysung Corp., Korea, from 2002 to 2005 and was a Research Professor with Myongjui University, Yongin, Korea, from 2005 to 2007. He was a Postdoctoral Research Associate with Trexas A&M University, College Station, in 2007 and an Assistant Professor with Chonnam National University, Kwangju, Korea, from 2007 to 2009. His research interests are the protection, control, and automation of power systems.

Jong-Young Park received the B.S., M.S., and Ph.D. degrees from Seoul National University, Seoul, Korea in 1999, 2001, and 2007, respectively.

Currently, he is a Senior Researcher at Korea Electrotechnology Research Institute (KERI). His research interests include the system protection scheme (SPS), the control of reactive power, and IT applications to energy management systems.

Sang-Hee Kang (S'90–M'93) received the B.S., M.S., and Ph.D. degrees from Seoul National University, Seoul, Korea, in 1985, 1987, and 1993, respectively.

He is a Professor at Myongji University, Yongin, Korea. He was a Visiting Fellow and Visiting Scholar at the University of Bath, Bath, U.K., in 1991 and 1999. He has also been with the Next-Generation Power Technology Center, Korea, since 2001. He was an Honorary Academic Visitor at the University of Manchester, Manchester, U.K., during 2007. His research interest is to develop digital protection systems for power systems using digital signal processing techniques.

Mladen Kezunovic (S'77–M'80–SM'85–F'99) received the Dipl. Ing., M.S., and Ph.D. degrees in electrical engineering in 1974, 1977, and 1980, respectively.

He is the Eugene E. Webb Professor and Site Director of the Power Engineering Research Center (PSerc), an NSF I/UCRC at Texas A&M University, College Station. He worked for Westinghouse Electric Corp., Pittsburgh, PA, during 1979–1980 and Energoinvest Company, in Europe, during 1980–1986. He was Visiting Associate Professor at Washington State University, Pullman, in 1986–1987 and a Visiting Professor at the University of Hong Kong in the fall of 2007. His main research interests are digital simulators and simulation methods for relay testing, as well as application of intelligent methods to power system monitoring, control, and protection.

Dr. Kezunovic is a member of CIGRE and Registered Professional Engineer in Texas.